



OPEN Tuning the band gap, optical, mechanical, and electrical features of a bio-blend by Cr₂O₃/V₂O₅ nanofillers for optoelectronics and energy applications

Tarek I. Alanazi¹, Raghad A. Alenazi¹ & Adel M. El Sayed^{2✉}

This work presents a facile approach for controlling the optical and electrical parameters of a biopolymeric matrix for optoelectronics. Vanadium oxide (V₂O₅) and chromium oxide (Cr₂O₃) nanoparticles (NPs) were prepared and incorporated into the carboxymethylcellulose/polyethylene glycol (CMC/PEG) blend by simple chemical techniques. Transmission electron microscopy (HR-TEM), and X-ray diffraction (XRD) data showed that V₂O₅ and Cr₂O₃ exhibited spherical shapes with sizes in the range of 40–50 nm and 10–20 nm, respectively. In addition, the blend's degree of crystallinity was sensitive to the V₂O₅ and Cr₂O₃ doping ratios. The scanning electron microscopy (FE-SEM) and the elemental chemical analysis (EDAX) used to study the filler distribution inside the blend, and confirmed the existence of both V and Cr in the matrix. Fourier transform infrared (FTIR) spectroscopy showed that the dopants significantly affected the blend reactive (C–O–C, OH, and C=O) groups. The stress–strain curves illustrated the reinforcing effect of the dopants up to 1.0 wt% Cr₂O₃/V. The transmittance and absorption index spectra in the visible-IR wavelengths decreased with increasing filler content. Utilizing Tauc's relation and (optical) dielectric loss, the direct (indirect) band gap narrowed from 5.6 (4.5) eV to 4.7 (3.05) eV at 1.0 wt% Cr₂O₃/V. All films have an index of refraction in the range of 1.93–2.17. AC conductivity was improved with increasing filler content and temperature. The energy density at 50 °C is in the range of 1–3 J/m³. The influence of V₂O₅ and Cr₂O₃ content on the optical conductivity, dielectric constant, loss, and dielectric modulus of CMC/PEG was reported. These enhancements in electrical and optical properties, along with the potential for band gap engineering, offer promising prospects for advanced applications in optoelectronics and energy-related fields.

Keywords Cr₂O₃/V₂O₅ nanoparticles, CMC/PEG biopolymer blend, Band gap engineering, Energy density, Dielectric modulus, Stress–strain

Biopolymer nanocomposites (BPNC) are made by incorporating a tiny amount of inorganic nanofillers into a biopolymer matrix. Besides the simplicity in fabrication and handling, the key factors influencing the BPNC' properties for the targeted applications include the nature of the polymer matrix, filler composition, size, and quantity, and the homogeneity degree inside the BPNC^{1,2}. Blending at least two biopolymers is a simple and cost-effective approach for obtaining new materials with desirable characteristics that can't be obtained from a polymer³. Nano-sized materials in the form of nanoparticles (NPs) exhibit unique features owing to their reactivity, and huge surface area⁴. Loading NPs induces modifications in the blend's electronic structure and energy gap. Therefore, the resulted nanocomposites can be used as multifunctional materials for advanced technological applications such as optoelectronic devices, solar cells, light-emitting (organic) diodes, memory devices, image sensors, electrochemical, and energy-related uses^{1,3,5}.

The chemical versatility of carboxymethylcellulose (CMC, also known as cellulose gum) arises because it is a basic cellulose derivative that consists of Na carboxymethyl (CH₂COONa) attached to a polysaccharide (cellulose) backbone^{4,6}. CMC is semi-crystalline ionic-type cellulose ether, an environmentally friendly, biodegradable, and inexpensive polymer extract from the fibrous tissue of plants, fruit, and vegetable-based wastes^{7,8}. Owing to

¹Department of Physics, College of Science, Northern Border University, 73222 Arar, Saudi Arabia. ²Physics Department, Faculty of Science, Fayoum University, El-Fayoum 63514, Egypt. ✉email: ams06@fayoum.edu.eg

its exceptional viscosity, biocompatibility, flocculating property, high water absorption, thermal gelatinization, transparency, and ability to form a continuous medium, CMC can form flexible and strong films^{9,10}. These features made CMC the best choice as an adhesive, thickening agent, and stabilizer for improving the processing ability of textiles, cosmetics, paper, foodstuffs, creams, lotions, toothpaste compositions, and drug delivery^{10–15}. On the other side, poly(ethylene glycol), or PEG, exhibits low toxicity, and excellent water solubility¹⁶. In the blending process, PEG is usually used as a pores-forming agent to enhance the free volume in the matrix and to allow the chain segments more freedom to move and rotate^{17,18}.

The production and use of CMC-based edible films have become essential for food recycling and sustainability⁷. Salem et al.¹⁹ reported that adding 10 wt% polypyrrole to CMC raised the blend's refractive index (n) from 2.11 to 2.64 and greatly decreased the band gap (E_g). This made the blend ideal for advanced optoelectronics. With the addition of starch and cellulose nanocrystals, the mechanical features and viscoelastic behavior of CMC can also be changed to suit farming and packaging needs²⁰. A previous study reported that blending PEG with PVA improved the refractive index of anti-reflective coatings²¹. El Askary et al.⁶ improved the optical characteristics of CMC/PVA by forming Er_2O_3 NPs inside the blend utilizing the laser ablation technique. Menazea et al.¹² fabricated $\text{MoO}_3/\text{PEO}/\text{CMC}$ nanocomposites by a hydrothermal method and solution casting. According to Kodsangma et al.¹⁴, the ionic interaction and physical cross-linking of OH with Zn^{2+} in $\text{ZnO}/\text{CMC}/\text{thermoplastic starch}$ improved its thermal, mechanical, and water resistance. The optical parameters of PVA/CMC/PEG modified with $\text{Zn}_{0.9}\text{Cu}_{0.1}\text{S}$ and $\text{Zn}_{0.95}\text{V}_{0.05}\text{S}$ were reported in Ref.^{9,16}. The energy density and dielectric moduli of PVC/PEG changed irregularly with increasing CeO_2 NPs content¹⁸. According to El-naggar et al.²², PVP/CMC mixed with 5.0 wt% hydrogen titanate nanotubes/tetramethylammonium iodide could be used in optoelectronics. Al-Muntaser et al.^{13,23} studied the band gap structure, dielectric moduli, and impedance of a CMC/PVA/PVP mixed with ZnO or TiO_2 NPs. Farea et al.²⁴ improved the semiconducting properties of PVA/CMC by introducing CdO NPs.

Among the transition metal oxides as nanofillers, the rhombohedra chromium oxide (Cr_2O_3) is a stable material with p -type, wide E_g (3.1–3.4 eV), mobility of $0.14 \text{ cm}^2 \text{ V}^{-1} \text{ s}^{-1}$, and high energy density¹⁰. Therefore, Cr_2O_3 is suitable for photonics, optical storage devices, nanolasers, and also as a cathode material^{25,26}. Additionally, the limited size and high density of corner/edge sites give the nano-sized vanadium oxides a distinctive geometry²⁷. Vanadium pentoxide (V_2O_5) exhibits a V^{5+} oxidation state and acts as a semiconductor of n -type, a relatively narrow E_g (1.9–2.3 eV) and exceptional thermoelectric and electrochromic features. In addition, it has been used effectively in diverse fields such as gas sensing, photocatalysis, energy storage, and supercapacitors^{28,29}. The simultaneous doping with two transition metal oxides can provide composites with interesting biological features for biomedical or clinical applications³⁰. El-Morsy et al.^{2,11} investigated the opto-electrical features of $\text{CdO}/\text{Al}_2\text{O}_3/\text{CMC}$ and $\text{Cr}_2\text{O}_3/\text{TiO}_2/\text{CMC}$ composites. Gaabour³¹ studied the dielectric characteristics of $\text{Cr}_2\text{O}_3/\text{CMC}/\text{PEO}$ nanocomposites. Hamza and Habeeb loaded $\text{SiO}_2/\text{Cr}_2\text{O}_3/\text{PVA}/\text{CMC}$ nanocomposites and proposed their use as antimicrobial films for the food industry¹⁰. Menazea et al.²⁷ reported improved antibacterial efficacy for the chitosan/PVA with increasing V_2O_5 NPs content. Awwad et al.³² reported that V_2O_5 NPs created by laser ablation inside PEO/chitosan matrix changed the band gap and conductivity of the blend in a non-monotonic behavior with increasing ablation time.

The literature survey revealed that no complete reports are found on $\text{Cr}_2\text{O}_3/\text{V}_2\text{O}_5/\text{CMC}/\text{PEG}$ bio-nanocomposites. Our focus and interests are to combine the unique features of V_2O_5 , Cr_2O_3 , and CMC/PEG in composites, and explore the influence of simultaneous doping with V_2O_5 and Cr_2O_3 on the structural features, interactions, and physical characteristics of the CMC/PEG blend. The results revealed that $\text{Cr}_2\text{O}_3/\text{V}_2\text{O}_5$ can tune and engineer the blend structure, mechanical, optical, and electrical properties. This encourages the use of prepared flexible nanocomposites for some optoelectronic and energy-storing devices.

Experimental section

Chemicals, methodology, and free-standing composite film fabrication

Chromium (III) acetate [$\text{Cr}(\text{C}_2\text{H}_3\text{O}_2)_3$, 229 g/mol, Med Chem Express, USA], vanadium (V) oxide [V_2O_5 , 181.18 g/mol, Merck], HCl, oxalic acid [$\text{C}_2\text{H}_2\text{O}_4 \cdot 2\text{H}_2\text{O}$, 126 g/mol], carboxymethylcellulose [CMC, $(\text{OCH}_2\text{COONa})_y\text{C}_6\text{H}_7\text{O}_2(\text{OH})_x]_n$, ($y+x=3$), 0.29×10^6 g/mol, El Nasr Pharmaceutical Chemicals Co., Egypt] and polyethylene glycol [PEG, $\text{H}(\text{OCH}_2\text{CH}_2)_n\text{OH}$, 6000 g/mol, DOP Organic Kimya, Konya, Turkey]. Distilled water was used as a solvent.

V_2O_5 (1.1 g) was dissolved in HCl (30 ml) by stirring for 30 min. The obtained solution was heat-treated at 100°C for 6 h. The green product was then dissolved in ethanol, dried, and then annealed at 400°C for 1 h to obtain V_2O_5 NP. $\text{Cr}(\text{C}_2\text{H}_3\text{O}_2)_3$ (1.15 g) and oxalic acid (0.63 g) were dissolved in pure water (25 mL) by stirring for 1.0 h/ 50°C . The sample was put in a furnace at 100°C to dry (remove the excess water). Then it was subjected to a thermal decomposition at $400^\circ\text{C}/1.0$ h to obtain solid Cr_2O_3 NPs.

CMC (0.9 g) was dissolved in distilled water (50 mL) by stirred at 85°C . PEG (0.1 g) was also dissolved in distilled water (10 mL) at RT. These dissolutions took 1.0 h to obtain transparent and clear CMC and PEG solutions. Then the two solutions were mixed and stirred for 1.0 h, at RT. The nanocomposite solutions were prepared following the same procedures with the addition of 0.5 wt% V_2O_5 , 0.5 wt% $\text{Cr}_2\text{O}_3/0.5$ wt% V_2O_5 , 1.0 wt% $\text{Cr}_2\text{O}_3/0.5$ wt% V_2O_5 , and 2.0 wt% $\text{Cr}_2\text{O}_3/0.5$ wt% V_2O_5 to the blend solution. These fillers' contents were calculated using the relation: $x(\text{wt}\%) = \frac{m_f}{m_f+1} \times 100\%$, where m_f is the mass of the filler (V_2O_5 or $\text{Cr}_2\text{O}_3/\text{V}_2\text{O}_5$) and the "1" is the mass of the polymers. The uniformly mixed blend and nanocomposite solutions were poured into Petri dishes (glass) and left for more than 24 h to dry in a controlled environment at $40\text{--}45^\circ\text{C}$.

Devices and characterization

The structure and morphology of the fillers (V_2O_5 , Cr_2O_3) were performed using field emission SEM, model Carl ZEISS (Sigma 500 VP), and TEM (JEM 2100, Jeol, Japan). A diffractometer (PANalytical/X'Pert/PRO) with copper K_α lines of wavelength $\lambda = 0.154$ nm, and step 0.02° was used to study the crystal and phases of V_2O_5 and Cr_2O_3 , CMC/PEG and BPNC films. The films' morphology explored using FE-SEM. FTIR spectra were collected in $4000\text{--}400$ cm^{-1} wavenumbers, using a Bruker/vertex70 spectrophotometer. Stress vs. strain (i.e., tensile testing) was obtained utilizing a testing machine of ZwickRoell, Z010 TN-Germany, operated at 1×10^3 N. The toughness was measured from the integrated area under the obtained curves using the Origin Pro software. The films of CMC/PEG and Cr_2O_3/V_2O_5 /CMC/PEG were cut in a specific shape (length and width of 8 cm and 1.5 cm, respectively), where the test was done three times for each sample at a speed of 50 mm/min. UV-Vis-NIR transmittance (T%) and absorption (Abs.) in 200–1400 nm wavelengths, were recorded by a Shimadzu spectrophotometer (UV-3600/UV/Vis/NIR). An accurate (± 0.001 mm) digital micrometer evaluated the sample thickness. All of these measurements were performed at RT. The dielectric features and parameters were considered using a broad-band dielectric spectroscopy (Novocontrol turnkey 40) System, across 10^{-1} Hz–10 MHz frequencies at different three temperatures (30, 50, and 70°C).

Results and discussion

Morphology and structure of the sol-gel-derived NPs

The morphology of the sol-gel-prepared V_2O_5 and Cr_2O_3 was checked by HR-TEM, as shown in Fig. 1a,b, and also FE-SEM, Supplementary Fig. S1a,b. See the supporting materials file. The powders are composed of NPs, and the size of V_2O_5 (Fig. 1a) is in the range of $\sim 40\text{--}50$ nm. Also, Cr_2O_3 exhibits more spherical particles, 10–20 nm in size. Figure 1a',b' shows a histogram of the particle size distribution of both V_2O_5 and Cr_2O_3 , respectively. Supplementary Figure S1a,b also shows a particle morphology for the powders. As observed in Fig. 1a,b, V_2O_5 NPs agglomerate and appear with a larger grain size. This NPs adhesion is due to covalent or metallic bonds which form micro-sized structures³³.

Figure 2 shows the XRD spectrum of Cr_2O_3 . Well-defined diffraction peaks appear at $2\theta = 24.45^\circ$, 33.55° , 36.25° , 41.48° , 50.29° , 54.85° , 63.62° , and 65.22° , which correspond to Bragg reflections of $(hkl) = (012)$, (104) , (110) , (113) , (024) , (116) , (214) , and (300) , respectively. This chart indicates the formation of Cr_2O_3 with rhombohedra structure, $R\bar{3}c$ SG, and parameters (lattice): $a = 4.957$ Å & $c = 13.584$ Å, is coincident with the data of JCPDS no.: 84-1616. The Sherrer's formula: $D = \frac{K \times \lambda_{Cu}}{FWHM \cdot \cos\theta}$, where $\lambda_{Cu} = 0.154$ nm, K is the Sherrer's constant (0.9), and $FWHM$ of the peak is the width at half maximum intensity, was used for the average crystallite size D determination, which was found in the order of ~ 25.36 nm. While FE-SEM measures the distances between

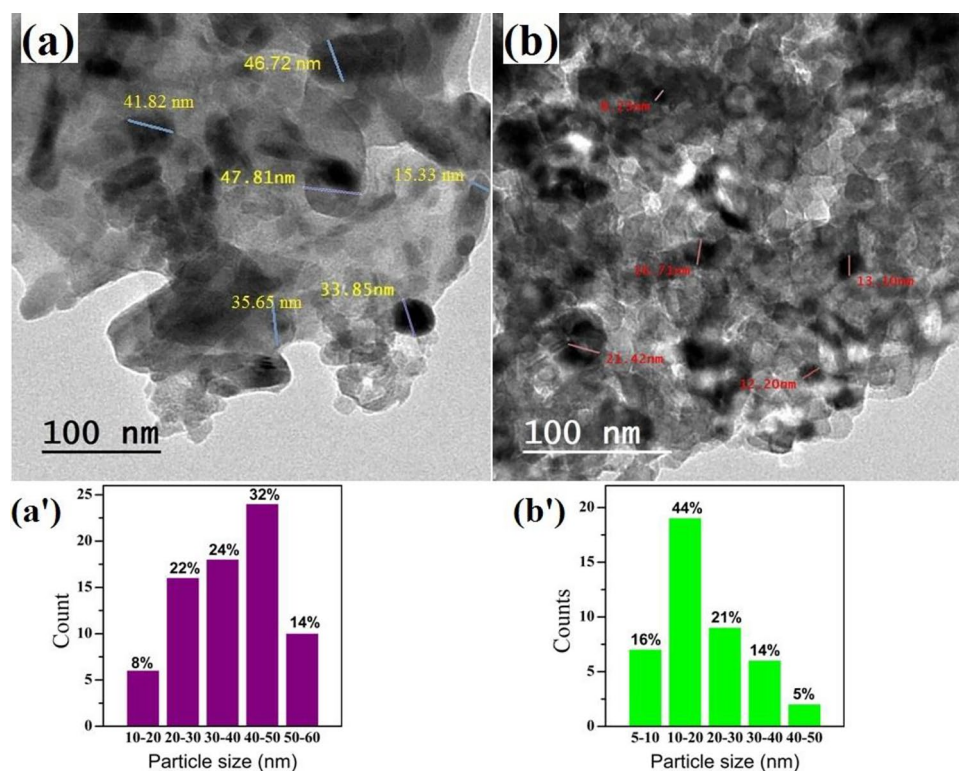


Figure 1. HR-TEM images for (a) V_2O_5 , (b) Cr_2O_3 NPs. (a',b') show the corresponding histogram particle size distribution.

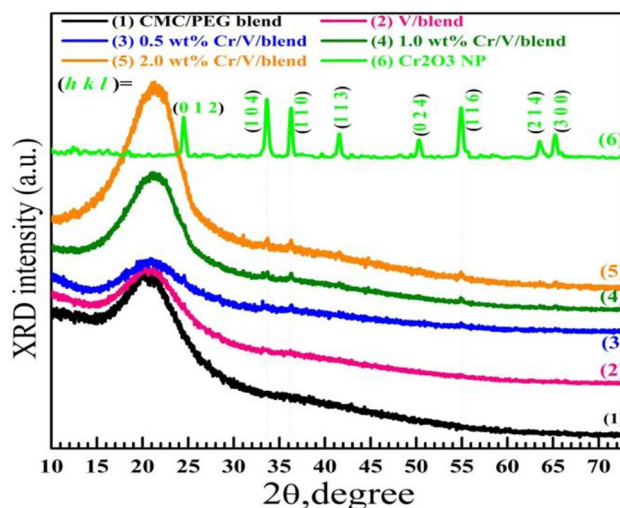


Figure 2. XRD charts of CMC/PEG blend, V_2O_5 /blend, Cr_2O_3/V_2O_5 /blend and Cr_2O_3 NP.

the grains (grain or particle size), XRD calculates D , which may represent a part of the grain³⁴. In addition, the XRD pattern of V_2O_5 is shown in Supplementary Fig. S2.

Structural and mechanical properties of the films

XRD was also employed to investigate the CMC/PEG blend structure and the roles of V_2O_5 and Cr_2O_3 in its structural characteristics. Figure 2 shows the patterns of virgin CMC/PEG, 0.5 wt% V_2O_5 /blend, and 0.5–2.0 wt% Cr_2O_3/V_2O_5 /blend. The pattern of the unfilled blend displays a broad peak in the region of $2\theta = 16$ – 27° with maximum intensity at $2\theta = 20.9^\circ$. The appearance of this peak indicates the semicrystalline structure of the blend, i.e., the blend has crystalline regions inside an amorphous phase. Already, the XRD chart of the CMC polymer contains a wide peak around $2\theta = 22.13^\circ$ ¹⁹. This wide peak is certainly overlapped with the characteristic one of PEG (at $2\theta = 19.5^\circ$ ¹⁶). This semicrystallinity originates because the hydrogen bonds between PEG and CMC force the chains to form arranged lamellas throughout the amorphous parts³⁵. A similar observation was noted for PVA/sodium alginate³⁶. Introducing 0.5 wt% V_2O_5 and codoping with 0.5 wt% Cr_2O_3 decreases the intensity of the main peak. The fillers (V_2O_5 and Cr_2O_3) and the reactive groups of the matrix should have interacted and caused this change, where the amorphous areas inside the matrix became predominant. In other words, this note indicates that the filler inside the blend degrades the ordered (lamella) structures and increases the films' amorphousness³⁷. It also indicates the good dispersion of these small amounts of the nanofillers inside the amorphous regions.

However, with increasing the Cr_2O_3 NPs content, all of the Cr_2O_3 peaks emerge instead of the one at $2\theta = 24.45^\circ$, which certainly overlapped with the wide peak of the blend. In addition, the main peak's intensity significantly increased and shifted to $2\theta \approx 21.2^\circ$. The nanofillers' interesting surface energy, which encourages particle aggregation when concentration increases, as shown in Fig. 3, may be responsible for this. Similarly, Alhazime¹⁵ detected the main halo peak of CMC/PVP modified with ZnS/NiO at 21.59° . The improvement in blend crystallinity may also be due to the local structural arrangements made by complex formation within the matrix. Raising the Cr_2O_3 content to 2.0 wt% led to this outcome. These results indicate the possible control of blend structure by inserting specific amounts of V_2O_5/Cr_2O_3 NPs¹¹.

Figure 3a shows the surface images for the films taken by FE-SEM. The films are homogenous, nonporous, and crack-free. The fillers are uniformly distributed on the blend surface and form clusters as their content increases beyond 0.5 wt% V_2O_5 . Also, the agglomerations are clearly presented in the 2.0 wt% Cr_2O_3/V -loaded film. The elemental chemical analysis for the blend filled with 0.5 wt% V_2O_5 and 2.0 wt% Cr_2O_3/V is depicted in Fig. 3b. The C and O are the main components of the CMC and PEG. Their peaks appear at 0.27 and 0.53 keV, respectively, arising from $K_{\alpha 1}$ emissions. The peak at ~ 1.05 keV is owing to $K_{\alpha 1}$ line of Na that is found in CMC. The peaks at ~ 4.95 and 5.40 keV confirm the presence of V in the 0.5 wt% V_2O_5 -loaded film. In addition, the Cr element displays three emissions at 0.55 keV (L_{α}), 5.4 keV (K_{α}), and 5.95 keV (K_{β}), respectively. Although XRD wasn't able to confirm the existence of V due to the small amount of added V_2O_5 and the detection limit of XRD, EDX spectra confirmed their presence.

Figure 4 displays the FTIR spectra of the blend and V_2O_5/Cr_2O_3 /blend films. The main vibrational frequencies in these spectra are distinguished as follows: (i) A wide peak at about 3300 cm^{-1} can be assigned to the O–H stretching in the blend. (ii) A minor peak at 2870 cm^{-1} related to the vibration of H–C (aliphatic). (iii) The peaks located at 1022, 1317, 1421, and 1596 cm^{-1} are owing to C–O–C and O–H bending, H_2C scissoring, and vibrations of C=O of COO[−] group, respectively^{11,20}. (iv) The vibrations of C–O stretching of ether groups are appearing at 1055 cm^{-1} and 1098 cm^{-1} . (v) Finally, the tiny peaks at 841 and 580 cm^{-1} are arising from the asymmetric rocking of CH_2 and the stretching in C–C, respectively⁶. All of these functional groups are found in the CMC/PEG blend's structure. The spectra of the Cr_2O_3/V_2O_5 /CMC/PEG films exhibit the same peaks but with

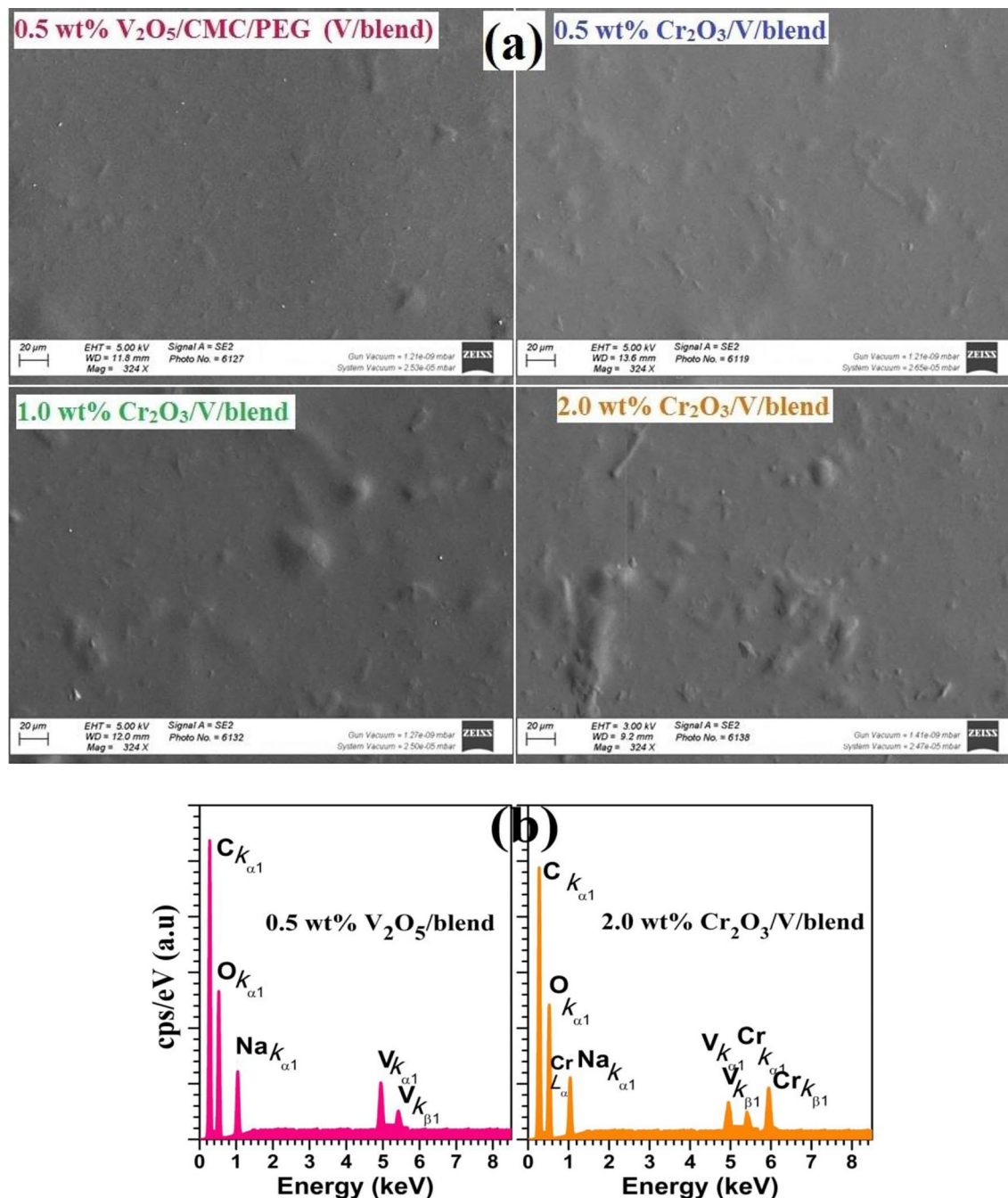


Figure 3. (a) FE-SEM images for 0.5 wt% V₂O₅/blend and 0.5–2.0 wt% Cr₂O₃/V/blend (scale bar: 20 μ m), (b) EDAX spectra of 0.5 wt% V₂O₅/blend and 2.0 wt% Cr₂O₃/V/blend.

reduced intensities compared to the blend. This suggests effective interactions between Cr₂O₃/V₂O₅ NPs and the blend molecules. The high tendency of OH to create charge-transfer complexes forces it to interact (physically) with V–O and Cr–O through chelating and the V₂O₅/Cr₂O₃ reinforcing effects³⁷. Some minor peaks, however, at 841 and 1098 cm⁻¹ appear with decreasing intensity at 0.5 wt% V₂O₅ and 0.5 wt% Cr₂O₃/V₂O₅ content, then their intensity enhances with increasing Cr₂O₃ NPs ratio to 2.0 wt%. In addition, the intensity of 1098 cm⁻¹ band shifted to 1105 cm⁻¹ at 2.0 wt% Cr₂O₃/V₂O₅ filler content. A similar result was reported for PEO/CMC modified with MoO₃ nanoblets¹². No new bands are observed in FTIR spectra of V₂O₅ and V₂O₅/Cr₂O₃-doped films. This confirms the physical interactions between these nanofillers and blend molecules¹¹.

The stress–strain curves of the films are shown in Fig. 5, and the values of the mechanical parameters (σ_M , ϵ_M , σ_B , ϵ_B , and toughness) of the films are summarized in Table 1. The blend has $\sigma_M = 9.75$ MPa which is consistent with the value reported for CMC (10.33 MPa)⁸. The values of σ_M , ϵ_M , σ_B and ϵ_B for CMC/PEG were improved slightly after filling with 0.5 wt% and 1.0 wt% Cr₂O₃/V₂O₅ NPs. Similarly, σ_M of CMCS was improved after loading 10 wt% boehmite NPs¹. The enhanced surface area of the added nanosized materials improves the interfacial

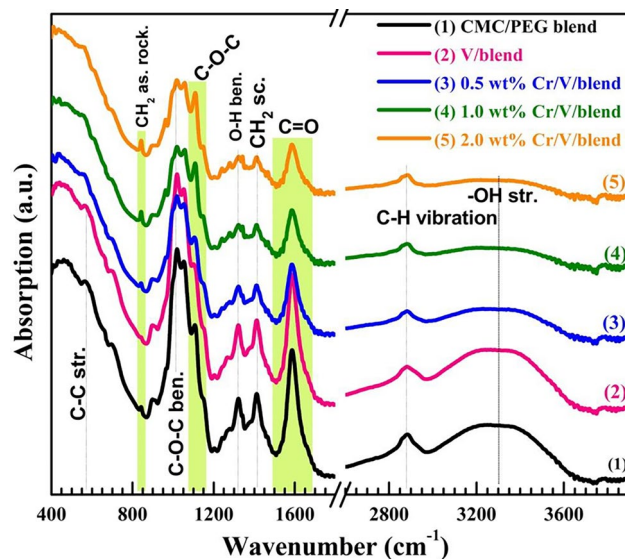


Figure 4. FTIR spectra of the blend, V_2O_5 /blend, and Cr_2O_3/V_2O_5 /blend nanocomposites.

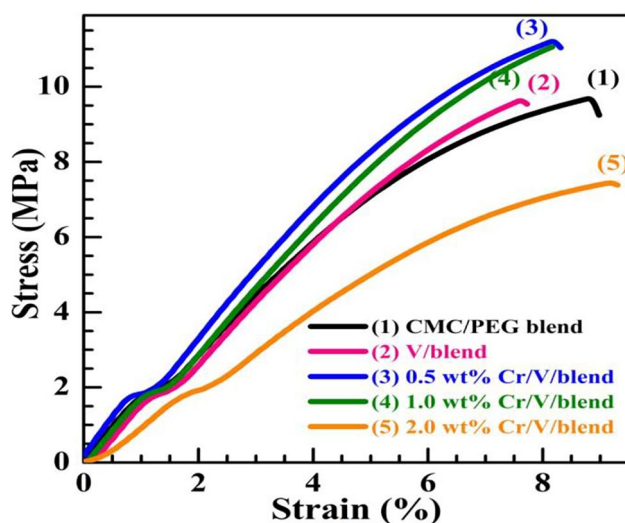


Figure 5. The tensile testing of the films.

Toughness (MPa)	ϵ_B (%)	σ_B (MPa)	ϵ_M (%)	σ_M (MPa)	Film composition
130.6 ± 43	9.0 ± 2.0	9.2 ± 2.8	8.8 ± 1.9	9.75 ± 1.4	CMC/PEG (blend)
111.2 ± 14.0	7.8 ± 1.4	9.5 ± 5.3	7.6 ± 2.0	9.65 ± 1.8	0.5 wt% V_2O_5 /blend (V/blend)
144.6 ± 10.4	8.35 ± 0.9	11.0 ± 4.7	8.2 ± 1.5	11.25 ± 2.6	0.5 wt Cr_2O_3 /V/blend
132.3 ± 12.5	8.2 ± 0.9	11.0 ± 2.6	8.2 ± 1.4	11.0 ± 1.9	1.0 wt Cr_2O_3 /V/blend
107.5 ± 9.5	9.3 ± 2.8	7.4 ± 2.6	9.2 ± 1.3	7.5 ± 1.4	2.0 wt Cr_2O_3 /V/blend

Table 1. Mechanical parameters (mean ± standard error) of the films: σ_M (tensile strength), ϵ_M (strain at σ_M), σ_B (stress at break), ϵ_B (strain at break), and toughness.

area between the blend chains and these fillers. This simplifies transfer of the stress from the blend to the filler via the created interfaces and, hence, improves the σ_M . The decrease in σ_M at 2.0 wt% Cr_2O_3/V_2O_5 arises from the agglomeration of fillers in the blend and the majority of the amorphous phase in the blend structure³⁸. This agglomeration and the resulting decrease in σ_M were the reasons for limiting the filler level to 2.0 wt%. The ϵ_B was reduced by doping with 0.5 wt% V_2O_5 then slightly increased with 1.0 wt% Cr_2O_3 NPs, but still smaller than

that of the pure blend. The restriction of the mobility of the polymer chain after nanofiller insertion confirms their reinforcement effect. These reinforced, flexible, and lightweight films are needed for various everyday uses, such as electronic equipment.

UV/vis–NIR spectra and optical features

The optical absorption/transmittance spectra were recorded and studied to verify the applicability of the $\text{Cr}_2\text{O}_3/\text{V}_2\text{O}_5/\text{CMC}/\text{PEG}$ films in optoelectronic applications. Figure 6a shows the absorption index (k) spectra that were determined from the recorded absorption (Abs.) and the incident wavelength (λ) as: $k = \frac{\text{Abs.} \cdot \lambda^{18}}{4d\pi}$. The film thickness (d) is given in Table 2, and $\frac{\text{Abs.}}{d} = \alpha$ (the absorption coefficient). All films have small k ($< 10^{-3}$) in the studied wavelength range. All nanocomposites exhibit higher k values relative to the blend. In the range $\lambda = 200\text{--}500$ nm, the 0.5 wt% $\text{Cr}_2\text{O}_3/\text{V}_2\text{O}_5/\text{blend}$ exhibits the highest value of k . At $\lambda > 600$ nm, the values of k increase with the fillers' content. New peaks are seen at ~ 400 and 620 nm in the k spectra of CMC/PEG blends containing Cr_2O_3 NPs and they are attributed to the SPR or surface plasmon resonance of Cr_2O_3 NPs. Such phenomenon indicates the interesting optical features of the BPNC films and can be exploited in applications related

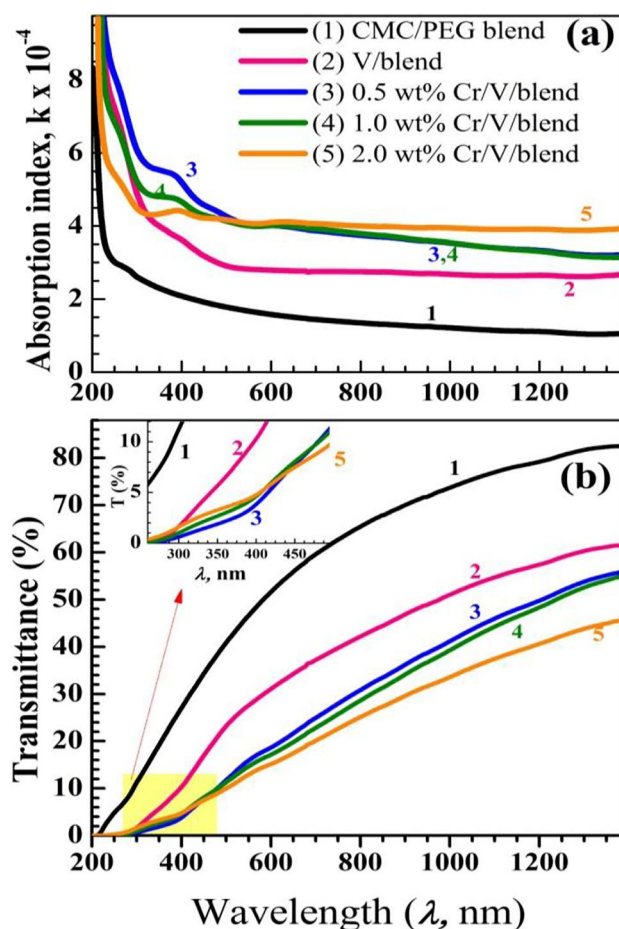


Figure 6. (a) absorption index spectra and (b) %transmittance of the films.

E_g^{loss} (eV)	n	E_g^i (eV)	E_g^d (eV)	T (%)	d (mm)	Film composition
5.20	1.93	4.50	5.60	59.6	0.18	CMC/PEG (blend)
4.40	2.08	2.80	4.50	37.2	0.16	0.5 wt% $\text{V}_2\text{O}_5/\text{blend}$ (V/bblend)
4.10	2.17	2.50	4.00	24.9	0.15	0.5 wt $\text{Cr}_2\text{O}_3/\text{V}/\text{blend}$
4.70	2.05	3.05	4.70	22.8	0.19	1.0 wt $\text{Cr}_2\text{O}_3/\text{V}/\text{blend}$
4.90	1.97	3.80	5.20	20.1	0.16	2.0 wt $\text{Cr}_2\text{O}_3/\text{V}/\text{blend}$

Table 2. Film thickness (d), optical transmittance ($T\%$) at 700 nm, direct and indirect band gap (E_g^d and E_g^i), index of refraction (n), and band gap from $\epsilon_{\text{loss}}^{\text{op}}$.

to some optoelectronic systems and sensors¹¹. The %transmittance values are depicted in Fig. 6b. The 0.5 wt% Cr₂O₃/V₂O₅/blend displays the lowest T% till $\lambda \approx 420$ nm, see the inset. At higher λ , T (%) falls with raising the fillers content. For comparison purposes, T% values at 700 nm wavelength are inserted in Table 2. The added NPs act as scattering points which are able to reflect/absorb the incident radiation. The blend and nanocomposites show T in the range of 45–82%, which is suitable for many uses and applications.

The possible optical transition and band gap (E_g) of the films can be investigated considering Tauc and Davis–Mott relations: $(\alpha hv)^2 = A(hv - E_g^d)$ and $(\alpha hv)^{1/2} = B(hv - E_g^i)$ for the allowed transitions (direct and/or indirect), where hv is incident energy, A and B are constants, and E_g^d and E_g^i are the direct and indirect E_g . The plots of $(\alpha hv)^2$ vs. hv and $(\alpha hv)^{1/2}$ vs. hv are illustrated in Fig. 7a,b. The nanocomposite films' E_g^d (E_g^i) values decreased from 5.6 (4.5) eV to 4.0 (2.5) eV upon loading 0.5 wt% Cr₂O₃/0.5 wt% V₂O₅. Similarly, V₂O₅ NPs created inside the chitosan/PVA by laser ablation reduced the E_g^d of the blend from 5.72 to 3.72 eV²⁷. Incorporating MoO₃ nanofillers (2.0–8.0 wt%) has reduced E_g^d (E_g^i) of CMC (80%)/PEO(20%) blend from 5.1 (3.2) eV to 3.24 (1.65) eV¹². The observed decrement in E_g^d (E_g^i) is assigned to the strong interaction of the host matrix with the fillers which produce defects and localized states inside the CMC/PEG gap and change the disorder degree of the host blend.

In addition, this decrement may result because the fillers can form a connected network in the structure of the blend and simplify the charge-carriers motion^{9,12}. In the literature, it was reported that adding of 10 wt% Zn_{0.9}Cu_{0.1}S to the blend composed of PVA (0.7)/CMC (0.15)/PEG (0.15) shrink its E_g^d (E_g^i) from 5.87 (5.31) eV to 4.47 (3.65) eV⁹. In addition, loading 6.0 wt% CdO NPs inside PVA/CMC matrix has reduced its E_g^d (E_g^i) from 5.65 (4.57) eV to 5.07 (3.91) eV²⁴. However, at 2.0 wt% Cr₂O₃/V₂O₅, a widening of E_g^d (E_g^i) to 5.2 (3.8) eV is observed. This blue shift may have happened due to NPs agglomeration and improving the ordering and crystallinity inside the blend, as seen from the XRD patterns of the samples. Similarly, doping with 0.5–1.5 wt% TiO₂ NPs has reduced the E_g^d (E_g^i) of the PVA/PVP/CMC blend from 5.43 (4.97) eV to 5.27 (4.72) eV, then they increased

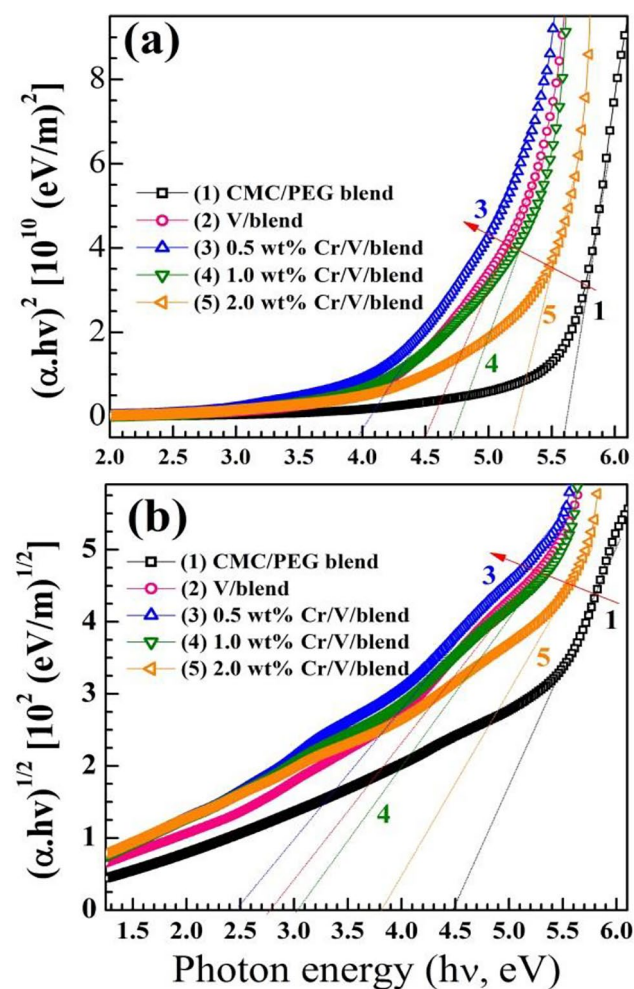


Figure 7. (a) E_g^d and (b) E_g^i of the films.

to 5.34 (4.77) eV at 3.0 wt% TiO₂ loading²³. In contrast, loading 0.1 wt% SrTiO₃/carbon nanotubes widened the E_g^d (E_g^i) of the polyvinylidene from 5.56 (5.27) eV to 5.70 (5.50) eV. Further increase in the filler level to 0.7 wt% decreased E_g^d (E_g^i) of the polymer to 5.53 (5.3) eV⁵. These observations make it possible to tune or engineer the E_g^d and E_g^i for various optoelectronic and electrochemical applications such as photocatalysis, solar cells, and sensors.

The index of refraction (n) is an essential parameter for design of the optical device. The n values were derived from the E_g^d using the relation: $\frac{n^2-1}{n^2+2} = 1 - \sqrt{\frac{E_g^d}{20}}$ ³⁹, see Table 2. As can be noted, the behavior of n with doping is the reverse to that of E_g values. The n value increased from 1.93 to 2.17 and this means that the films' reflectivity is improved, where the fillers act as scattering points. A similar finding was reported by Menazea et al.²⁷ where the laser-induced V₂O₅ increased n of chitosan/PVA from 2.13 to 3.32. NPs The dielectric loss ϵ_{loss}^{op} can be derived from n values and k spectra as $\epsilon_{loss}^{op} = 2nk$ ⁴⁰. Figure 8a shows the behavior of ϵ_{loss}^{op} with $h\nu$, as an alternative model to Tauc and Davis–Mott relation for estimating the E_g value⁴¹. ϵ_{loss}^{op} shows the role of the photon energy in the transition of the electrons. Extending the linear portions in the ϵ_{loss}^{op} plots the $h\nu$ axis can be used to obtain the E_g^{loss} values, as listed in Table 2. The E_g^{loss} also decreases from 5.2 to 4.1 eV at 0.5 wt% Cr₂O₃/0.5 wt% V₂O₅ content, then increases to 4.9 eV at 2.0 wt% Cr₂O₃/0.5 wt% V₂O₅, which is consistent with the change in E_g^d . Therefore, the E_g^{loss} and Tauc and Davis–Mott model can be used effectively to evaluate the E_g . A similar consistency between the two approaches was reported for PVA/PEG solid polymer electrolyte films⁴⁰ and AlPO₄/PVA/PEO blend⁴².

The optical conductivity (σ_{op}) of the can be determined from the relation⁴³: $\sigma_{op} = \frac{\alpha n c}{4\pi}$, where c is the speed of light. Figure 8b shows the curves of σ_{op} . vs. $h\nu$. All filled films exhibit enhanced σ_{op} . in comparison with the unfilled blend. Moreover, the σ_{op} . values enhanced with filler loading till 0.5 wt% Cr₂O₃/V₂O₅. It increases linearly with $h\nu$ till ~ 3.0 eV, and then the increase is slowdown. At $h\nu > 5.0$ eV, the UV photons cause a sharp increase in σ_{op} . values by exciting the charge carriers (electrons) to take part in the conduction process⁴⁴.

Electrical and dielectric features of nanocomposite films

AC conductivity

The BPNC' conductivity depends on the polymer's polarity, chemical nature of the fillers, doping ratio, particle size, dispersion, and the interfacial interactions between the chains of the polymer with the loaded particles⁴. Figure 9a–c shows the variation of σ_{ac} with the applied f , Log (σ_{ac}) vs. Log (f), at different temperatures (30, 50 and

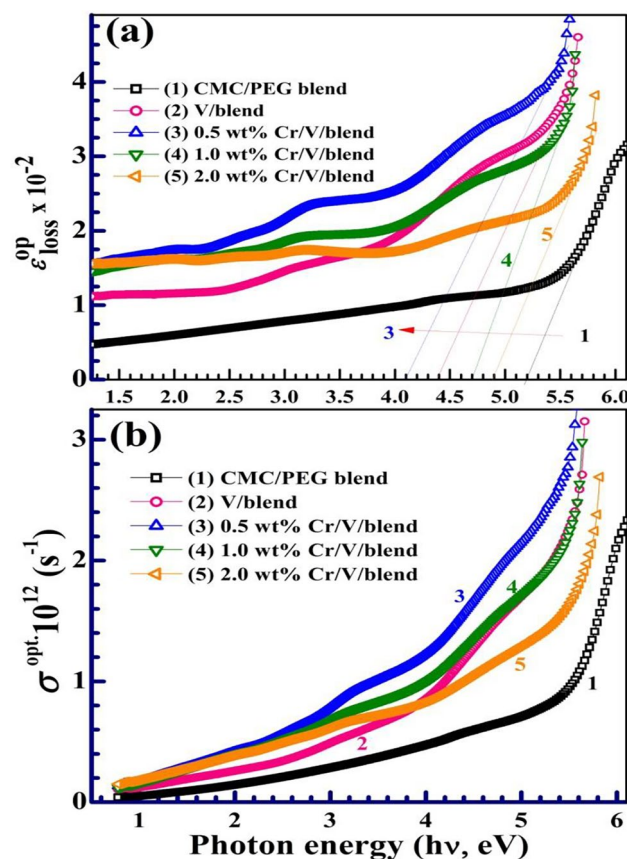


Figure 8. a,b Optical dielectric loss (ϵ_{loss}^{op}) and the optical conductivity of the samples.

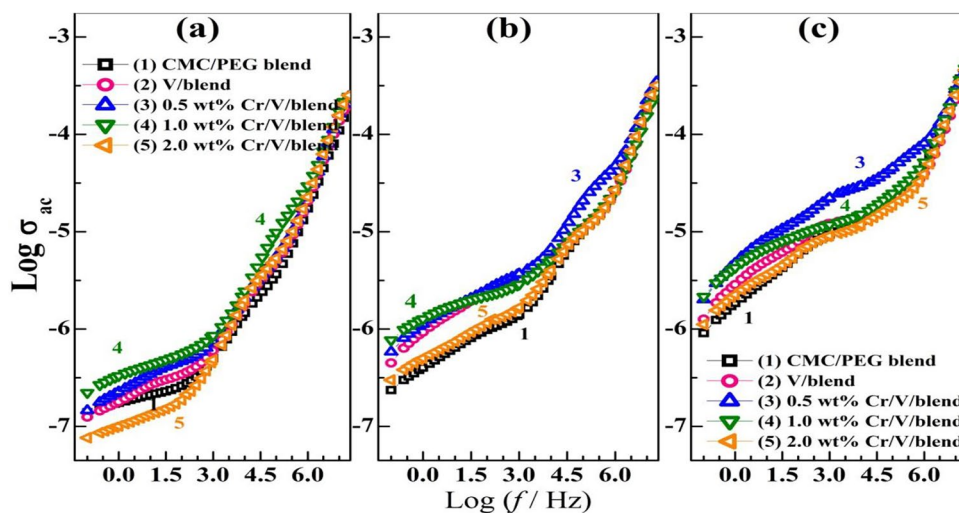


Figure 9. (a–c) Dependence of the ac conductivity on f for CMC/PEG, V_2O_5 /blend, and Cr_2O_3/V_2O_5 /blend at temperatures of (30, 50, 70 °C).

70 °C). The dispersion of σ_{ac} at low f is assigned to the interiorizations or spatial charges¹¹. The σ_{ac} of the CMC/PEG films is improved after loading the NPs till specific concentration of Cr_2O_3 , (1.0 wt% Cr_2O_3 at 30 °C, and 0.5 wt% Cr_2O_3 at 50 and 70 °C) where the Cr_2O_3 molecules can connect the gaps among the localized states and facilitate or simplify the charge carrier mobility. The increment of the amorphous portion throughout the blend after NPs incorporation as seen from the XRD results, the uniform distribution of the fillers, and the interfacial polarization among the chains of the blend and V_2O_5/Cr_2O_3 improve the films' conductivity. At 2.0 wt% Cr_2O_3/V_2O_5 , the agglomeration of the NPs reduces the interaction zone with the blend, and alters the charge carrier and defect numbers at the film surface due to the interactions among the Cr_2O_3/V_2O_5 NPs inside the matrix⁴⁵. Consequently, a substantial decrement of the interfacial polarization. Similar observations were noted in the system of carboxymethyl chitosan/cashew gum filled with boehmite NPs¹, and CMC/PEO loaded with $TiO_2/MWCNT$ ⁴⁶.

The σ_{ac} is almost f -independent at lower f regions and increases rapidly above 10^3 Hz which means that σ_{ac} obeys Jonscher's power relation: $\sigma(\omega) = \sigma_{dc} + A\omega^s$, where σ_{dc} , A and s are the conductivity at $f = 0$, a constant, and frequency exponent factor, respectively, and $\omega = 2\pi f$. This can be assigned to the hopping of charge carriers that acquire sufficient energy with increasing f and can hop through the conducting clusters and overcome the resistive grain boundaries⁴⁷. In addition, the σ_{ac} values at a certain value of f increase with heating from 30 to 70 °C, where the charge carrier mobility affected by the provided thermal energy. Also, the transit sites number increases with heating. Hence, the excited charge carriers can move through the matrix and overcome the energy barrier and take part in the conduction process⁴⁸. Similarly, at 10 kHz, the σ_{ac} of CMCS nanocomposites increased from about 0.4×10^{-5} at 30 °C to 0.34×10^{-4} S/cm at 90 °C¹. The enhancement in the blend conductivity after filling with V_2O_5/Cr_2O_3 , and with increasing f and temperature make the nanocomposite films more relevant for potential applications, including the optoelectronic devices and solid-state batteries.

Dielectric constant, loss, and energy density

The charge storage capacity can be determined through the dielectric permittivity analysis. The dielectric permittivity: $\epsilon^* = \epsilon' - j\epsilon''$, where ϵ' and ϵ'' represent the dielectric constant (the ability of the materials to store the energy due to all possible polarizations) and the dielectric loss (the energy dissipated in each cycle of applied f), respectively. The interfacial and dipolar polarizations are present in the unfilled matrix because it comprises a lot of polar groups and its constituents are of different conductivities. Figures 10 and 11 display the spectra of ϵ' and ϵ'' for CMC/PEG, V_2O_5 /blend and Cr_2O_3/V_2O_5 /blend at three different temperatures; 30, 50, and 70 °C. Both ϵ' and ϵ'' display the same behavior with f ; a fast decrement with f and are small or steady in the higher frequency region (f -independent).

These figures illustrate that a non-Debye type of behavior, where the space-charge accumulation is the reason behind the higher value of ϵ' at the lower f side without any relaxation peaks with increasing f . The large ϵ'' at low f is owing to the interfacial polarization (also known as Maxwell–Wagner–Sillars effect), where numerous charge carriers/dipoles have the time to be oriented in the alternative field direction, exhausting a significant energy value¹⁶.

The decrement of ϵ' and ϵ'' values as f increases is because the charge carrier and the chain segments can't follow the field due to the limited time. Therefore, the contribution of charge carriers to ϵ' with increasing f is diminished. Both ϵ' and ϵ'' are sensitive to the temperature and fillers' concentration. At 30 °C, their values increased with doping till 1.0 wt% Cr_2O_3 NPs. This could be attributed to that the interactions between V_2O_5 , Cr_2O_3 and CMC/PEG chains significantly affects the parallel ordering of the C–O–C, –OH, and C=O groups¹². Seemingly, it could be possible to fabricate electrochemical devices of high performance using these nanocomposite films. The observed decrease in ϵ' at filler concentration of 2.0 wt% Cr_2O_3/V_2O_5 may be explained in terms of

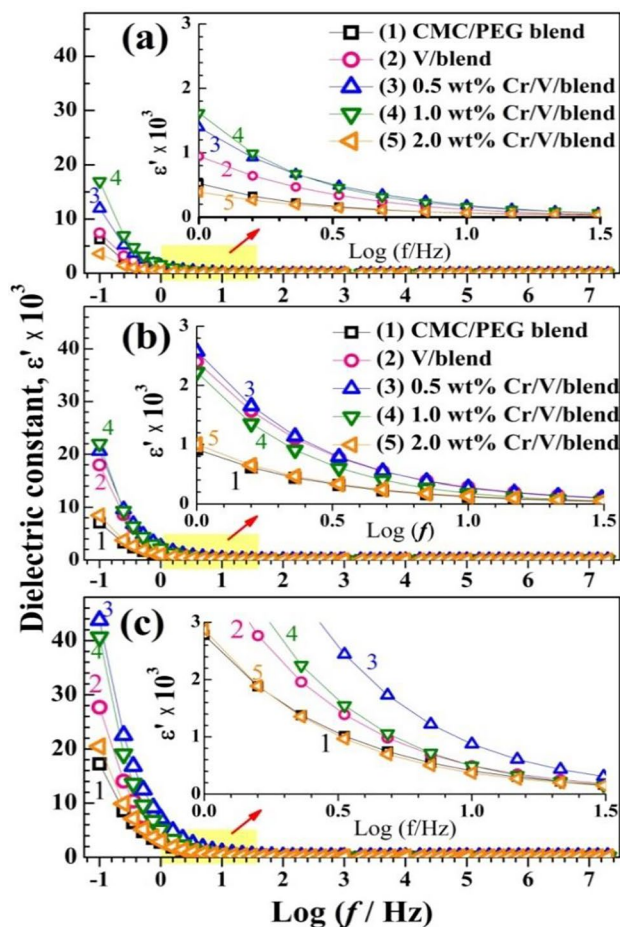


Figure 10. (a–c) Variation of ϵ' with f at temperatures of (30, 50, 70 °C).

the electrostatic interactions inside this heterogeneous structure which may result in a decrease in the interfacial polarization by creating microcapacitors and hence ϵ' reduced⁴⁹. Similar results were reported for $\text{Zn}_{0.95}\text{V}_{0.05}\text{S}/\text{CMC}/\text{PVP}/\text{PEG}$ ¹⁶ and $\text{ZnO}/\text{TiO}_2/\text{PEO}/\text{CMC}$ nanocomposites⁵⁰. The decrease in ϵ' values with increasing filler content beyond 0.5 wt% V_2O_5 and 0.5 wt% Cr_2O_3 is related to the decrement in σ_{ac} which is directly related to ϵ'' . Raising the temperature from 30 to 70 °C increases the supplied thermal energy to the blend system which can dissociate any coupled charges. In addition, the decrease of the polymer viscosity with heating facilitates the dipole/charge carrier motion to orient them in the field direction. This leads to intensifying the polarization and increasing the ϵ' ⁵¹.

The stored energy in a specific volume (energy density, U) is related ϵ' , free-space permittivity (ϵ_0), and the electric field (E) according to the relation: $U = \frac{1}{2}\epsilon_0\epsilon'E^2$ ²². Figure 12 shows U vs. $\text{Log}(f)$ for CMC/PEG loaded with V_2O_5 and $\text{Cr}_2\text{O}_3/\text{V}_2\text{O}_5$ at different temperatures. $U(f)$ of the blend increased upon doping with 0.5 and 1.0 wt $\text{Cr}_2\text{O}_3/\text{V}_2\text{O}_5$. The insets of Fig. 12 show the exponential decrease of U with f , but the U values significantly improved with heating. At very low f , U at 50 °C in the range of 1–3 J/m^3 and at 70 °C is in the range of 2–6 J/m^3 . The observed improvements in the U values make the doped blend best suitable for energy-related uses³.

Dielectric moduli and Argand plots

Supplementary Figure S3 and Fig. 13 display the dependence of the actual (M') and the (M'') fictitious modulus on f for the unfilled blend and $\text{Cr}_2\text{O}_3/\text{V}_2\text{O}_5/\text{blend}$ films at different temperatures. Both the two moduli display virtually very low value at lowest f values, which indicates that the charge carriers are constrained in the blend and that the effect of electrode polarization is minimized. M' displays a reverse behavior for ϵ' , so M' is the retro quantity of ϵ' ²³. M' grow linearly with f in the middle region of the applied frequencies and is nearly constant at higher f . This linear increase is owing to the charge carriers possess motilities of short range and the resulted conductivity²³. At 30 °C, M' decreases with increasing the fillers' content, this affirms the role of $\text{V}_2\text{O}_5/\text{Cr}_2\text{O}_3$ in the film's conductivity. Increasing the temperatures to 50 and 70 °C results in a decrement in the M' values. The observed relaxation peak in the M'' spectrum (Fig. 13) indicates a decent ionic conductivity contribution in the films¹². At 30 °C, the relaxation peaks in the M'' spectra shifted to a relatively higher f after doping with $\text{Cr}_2\text{O}_3/\text{V}_2\text{O}_5$ nanofillers. Also, the maximum peak lowered considerably with increasing the fillers content.

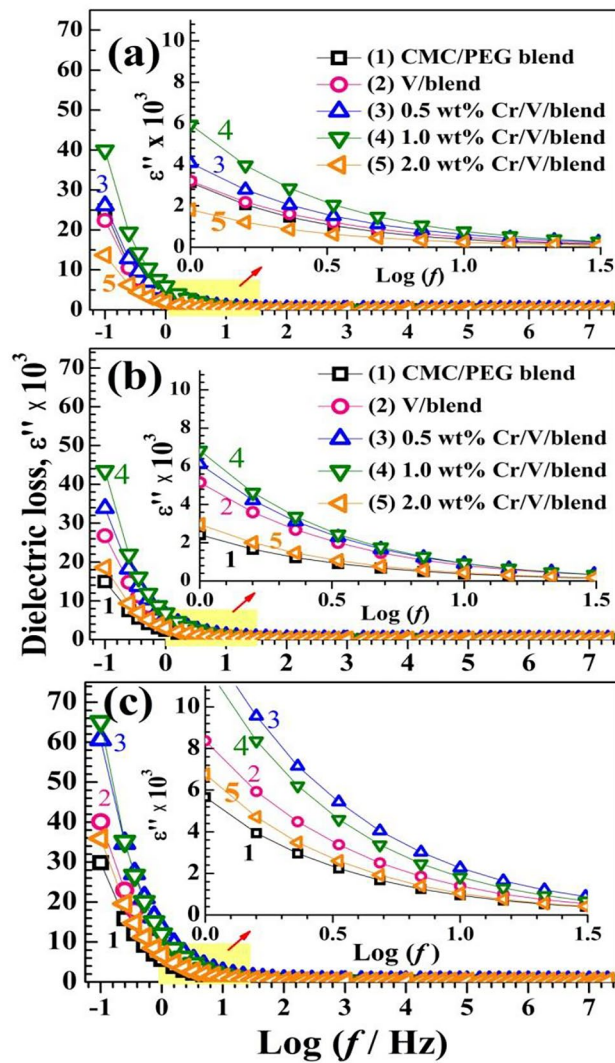


Figure 11. (a–c) Variation of ϵ'' with f at 30, 50, and 70 °C.

On the low f side of the relaxation peak, the ions can move over long distances by jumping among the neighbor sites. On the high f side of the peak, the charge carriers or ions can only move inside their wells. In other words, a phase transition occurred due to the change in dipole mobility from long to short ranges³¹. The dielectric relaxation time ($\tau \approx 1/(2\pi f_{\max})$) decreased from 1.6×10^{-5} s for the blend to 0.5×10^{-5} s for 2.0 wt% $\text{Cr}_2\text{O}_3/\text{V}_2\text{O}_5$ /blend film. At elevated temperatures, the relaxation peak position and intensity follow a non-monotonic trend with the fillers content.

The variation of M' vs. M'' is shown in Fig. 14, of CMC/PEG blend and nanocomposites display semicircles with centre positions not on the horizontal M' axis. This trend and the observed decrease in τ indicate the non-Debye type of the observed relaxation, which can be owing to the existence of relaxation mechanisms, various

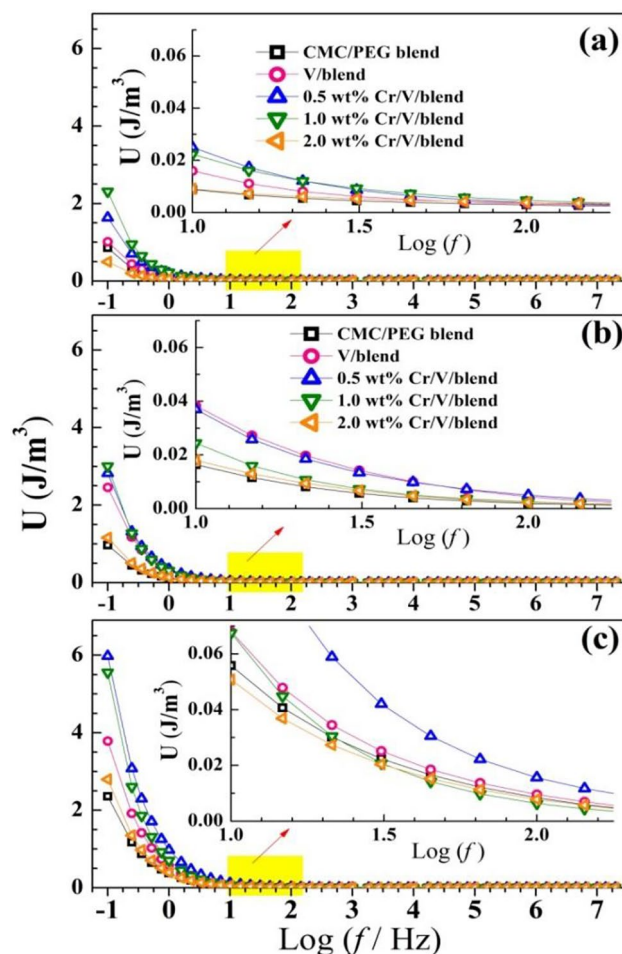


Figure 12. (a–c) Energy density of CMC/PEG, V_2O_5 /blend, Cr_2O_3/V_2O_5 /blend at temperatures of (30, 50, 70 °C).

types of polarization, and complex interactions among the dipoles and ions^{23,24}. At 30 °C, the semicircle diameters reduced with increasing the fillers content. Also, they increased significantly with heating the samples from 30 to 70 °C. The sample with the smaller diameter possesses the lowest resistance to the mobile charges^{52,53}. The observed single semicircles inside the blend and Cr_2O_3/V_2O_5 /blend nanocomposites denote singular relaxation⁶

Conclusion

Cr_2O_3/V_2O_5 /CMC/PEG BPNC was successfully prepared by chemical solution techniques. TEM/SEM analyses confirmed the nanostructuring of the fillers. XRD, FE-SEM and EDX analyses confirmed the successful doping with 0.5 wt% V_2O_5 and codoping with 0.5–2.0 wt% Cr_2O_3 NPs into the blend. The fillers tend to agglomerate when Cr_2O_3 NPs is 1.0 wt% or more. FTIR spectroscopy revealed the complexation and the physical interactions of the fillers with the reactive groups (C–O–C, OH, C=O) of the blend. This interaction and the uniform filler distribution improved the tensile strength from 9.75 to 11.25 MPa and the stress at break from 9.2 to 11 MPa. The Cr_2O_3 content of 0.5 wt% and 2.0 wt% showed a higher absorption index in the UV and IR regions, respectively.

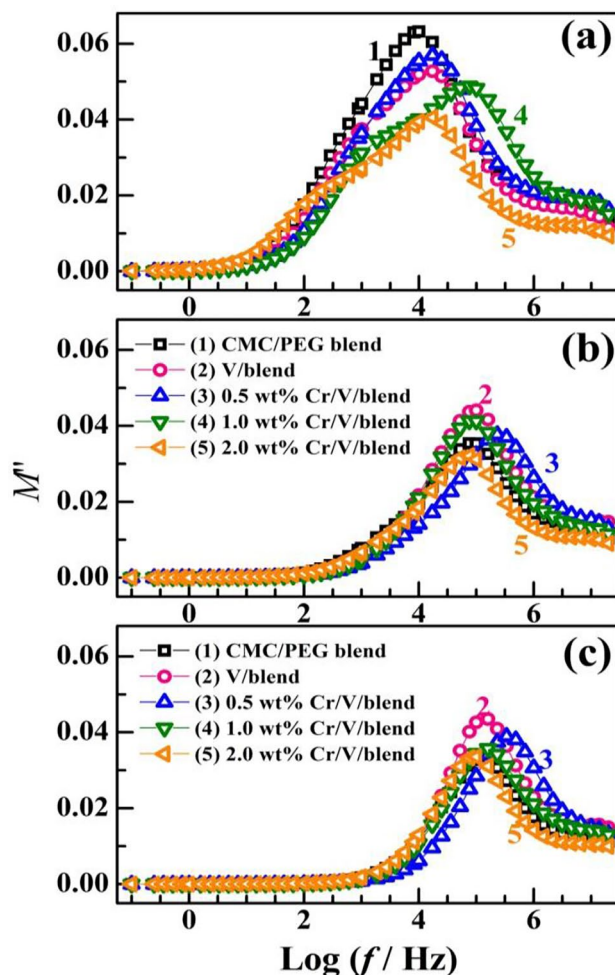


Figure 13. (a–c) Dielectric modulus M'' distribution of CMC/PEG blend and blend loaded with V_2O_5 , and Cr_2O_3/V_2O_5 NP at temperatures of (30, 50, 70 °C).

All films showed transmittance in the range of 45–82%. E_g^d (E_g^i) decreased from 5.6 (4.5) eV to 4.0 (2.5) eV at 0.5 wt% Cr_2O_3 , then increased to 5.2 (3.8) eV at 2.0 wt% Cr_2O_3 content. The E_g derived from ϵ_{loss}^{op} exhibited similar behavior as E_g^d . In addition, the index of refraction improved from 1.93 to 2.17. Both the optical and AC conductivities depended on the filler type and content. The dielectric constant, dielectric loss, and energy density were enhanced with Cr_2O_3 ratio of 1.0 wt% and also significantly improved with raising the temperature from 30 to 70 °C. The M'' spectra showed a relaxation peak of a non-Debye type. The Cole–Cole plots of CMC/PEG blend and nanocomposites displayed semicircles of reduced diameter as the temperature and filler content increased. The possible engineer or control of the optical features, mechanical properties, and the electrical properties by a certain amount of V_2O_5 and Cr_2O_3 makes these nanocomposites the best candidates for optoelectronics, sensors, and energy-related applications.

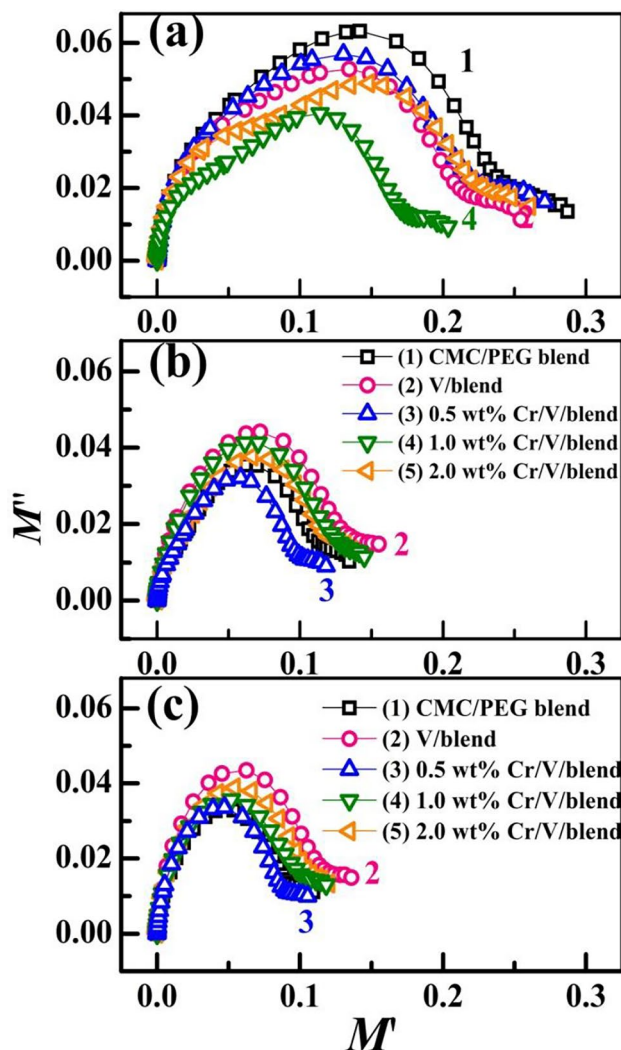


Figure 14. (a–c) M' vs. M'' curves of CMC/PEG blend and blend loaded with V_2O_5 , and Cr_2O_3/V_2O_5 NP at temperatures of (30, 50, 70 °C).

Data availability

The authors declare that all data generated or analyzed during this study are included in this published article and its supplementary materials file.

Received: 22 April 2024; Accepted: 20 May 2024

Published online: 31 May 2024

References

- Meera, K. & Ramesan, M. T. Tailoring the performance of boehmite nanoparticles reinforced carboxymethyl chitosan/cashew gum blend nanocomposites via green synthesis. *Polymer* **268**, 125706. <https://doi.org/10.1016/j.polymer.2023.125706> (2023).
- Alharbi, W. *et al.* Modification and development in the microstructure of carboxy methyl cellulose-TiO₂/Cr₂O₃ nanocomposites films for optoelectrical applications. *Inorg. Chem. Commun.* **159**, 111700. <https://doi.org/10.1016/j.inoche.2023.111700> (2024).
- El Sayed, A. M. Boosting the optical and electrical properties of PVA/Na-CMC blend by Cr₂O₃ nanoparticles for photonic and energy storage applications. *J. Energy Storage* **82**, 110609. <https://doi.org/10.1016/j.est.2024.110609> (2024).
- Morsi, M. A., Abdelaziz, M., Oraby, A. H. & Mokhles, I. Structural, optical, thermal, and dielectric properties of polyethylene oxide/carboxymethyl cellulose blend filled with barium titanate. *J. Phys. Chem. Solids* **125**, 103–114. <https://doi.org/10.1016/j.jpccs.2018.10.009> (2019).
- Taha, T. A. M., Alanazi, S. S., El-Nasser, K. S., Alshammari, A. H. & Ismael, A. Structure–property relationships in PVDF/SrTiO₃/CNT nanocomposites for optoelectronic and solar cell applications. *Polymers* **16**, 736. <https://doi.org/10.3390/polym16060736> (2024).
- El Askary, A. *et al.* Optical, thermal, and electrical conductivity strength of ternary CMC/PVA/Er₂O₃ NPs nanocomposite fabricated via pulsed laser ablation. *Phys. B* **637**, 413910. <https://doi.org/10.1016/j.physb.2022.413910> (2022).
- Yildirim-Yalcin, M., Tornuk, F. & Tokar, O. S. Recent advances in the improvement of carboxymethyl cellulose-based edible films. *Trend Food Sci. Technol.* **129**, 179–193. <https://doi.org/10.1016/j.tifs.2022.09.022> (2022).
- Dey, P. *et al.* Valorization of waste biomass for synthesis of carboxy-methyl-cellulose as a sustainable edible coating on fruits: A review. *Int. J. Biol. Macromol.* **253**, 127412. <https://doi.org/10.1016/j.ijbiomac.2023.127412> (2023).

9. El-naggar, A. M., Heiba, Z. K., Kamal, A. M. & Mohamed, M. B. Structural, dielectric, linear and nonlinear optical parameters of $Zn_{0.9}Cu_{0.1}S$ filled PVA/CMC/PEG blends. *Opt. Quant. Electron.* **55**, 790. <https://doi.org/10.1007/s11082-023-05085-0> (2023).
10. Hamza, R. S. A. & Habeeb, M. A. Reinforcement of morphological, structural, optical, and antibacterial characteristics of PVA/CMC bioblend filled with SiO_2/Cr_2O_3 hybrid nanoparticles for optical nanodevices and food packing industries. *Polym. Bull.* <https://doi.org/10.1007/s00289-023-04913-3> (2023).
11. El-Morsy, M. A., Awwad, N. S., Ibrahim, H. A., Farea, M. O. & Menazea, A. A. Fabrication of (Al_2O_3/CdO) metal and ceramic matrix composites reinforced CMC via laser ablation for optoelectronic applications. *Mater. Chem. Phys.* **312**, 128659. <https://doi.org/10.1016/j.matchemphys.2023.128659> (2024).
12. Menazea, A. A., Farea, M. O. & El-Khodary, S. A. Enhanced dielectric properties of α - MoO_3 nanobelts dispersed polyethylene oxide-carboxymethyl cellulose matrix-based nanocomposites. *Mater. Chem. Phys.* **312**, 128585. <https://doi.org/10.1016/j.matchemphys.2023.128585> (2024).
13. Al-Muntaser, A. A. *et al.* Tuning the structural, optical, electrical, and dielectric properties of PVA/PVP/CMC ternary polymer blend using ZnO nanoparticles for nanodielectric and optoelectronic devices. *Opt. Mater.* **140**, 113901. <https://doi.org/10.1016/j.optmat.2023.113901> (2023).
14. Kodsangma, A. *et al.* Mechanical properties and water resistance improvement of thermoplastic modified starch, carboxymethyl cellulose, and zinc oxide nanometal particles by reactive blending. *Int. J. Biol. Macromol.* **253**, 126783. <https://doi.org/10.1016/j.ijbiomac.2023.126783> (2023).
15. Alhazime, A. A. Effect of interchangeable proportions of ZnS and NiO nanoparticles on the optoelectronic and laser CUT-OFF filters properties of CMC/PVP blend. *J. Taibah Univ. Sci.* **17**(1), 2192848. <https://doi.org/10.1080/16583655.2023.2192848> (2023).
16. El-naggar, A. M., Heiba, Z. K., Kamal, A. M. & Mohamed, M. B. The incorporation of ZnS/V/TBAI in CMC/PVP/PEG blend to modify the structural, linear/nonlinear optical, and the electrical properties. *J. Mater. Sci. Mater. Electron.* **34**, 2125. <https://doi.org/10.1007/s10854-023-11550-z> (2023).
17. El Sayed, A. M. & Morsi, W. M. α - $Fe_2O_3/(PVA + PEG)$ Nanocomposite films; synthesis, optical, and dielectric characterizations. *J. Mater. Sci.* **49**, 5378–5387. <https://doi.org/10.1007/s10853-014-8245-9> (2014).
18. Heiba, Z. K. *et al.* Reinforcement of linear/nonlinear optical and dielectric characteristics of PVC/PEG blend based on $CeO_2/TBAI$ filler. *Inorg. Chem. Commun.* **158**, 111624. <https://doi.org/10.1016/j.inoche.2023.111624> (2023).
19. Salem, A. M., Mohamed, A. R., Abdelghany, A. M. & Yassin, A. Y. Effect of polypyrrole on structural, optical and thermal properties of CMC-based blends for optoelectronic applications. *Opt. Mater.* **134**, 113128. <https://doi.org/10.1016/j.optmat.2022.113128> (2022).
20. El Miri, N. *et al.* Bio-nanocomposite films reinforced with cellulose nanocrystals: Rheology of film-forming solutions, transparency, water vapor barrier and tensile properties of films. *Carbohydr. Polym.* **129**, 156–167. <https://doi.org/10.1016/j.carbpol.2015.04.051> (2015).
21. Mohammed, M. I. & El-Sayed, F. PEG's impact as a plasticizer on the PVA polymer's structural, thermal, mechanical, optical, and dielectric characteristics. *Opt. Quant. Electron.* **55**, 1141. <https://doi.org/10.1007/s11082-023-05420-5> (2023).
22. El-naggar, A. M., Heiba, Z. K., Kamal, A. M. & Mohamed, M. B. Structural, linear/nonlinear optical and electrical studies on PVP/CMC blend filled with hydrogen titanate nanotubes and TMAI. *Opt. Quant. Electron.* **55**, 1129. <https://doi.org/10.1007/s11082-023-05468-3> (2023).
23. Damoom, M. M. *et al.* The role of TiO_2 nanoparticles in enhancing the structural, optical, and electrical properties of PVA/PVP/CMC ternary polymer blend: nanocomposites for capacitive energy storage. *J. Sol-Gel Sci. Technol.* **108**, 742–755. <https://doi.org/10.1007/s10971-023-06223-6> (2023).
24. Farea, M. O. *et al.* Improving optical, electrical, and dielectric performance of PVA/CMC blend by incorporating cadmium oxide nanoparticles for energy storage applications. *J. Mater. Sci. Mater. Electron.* **34**, 2133. <https://doi.org/10.1007/s10854-023-11541-0> (2023).
25. Shahid, H., Arooj, I. & Zafar, S. Saba, Honey-mediated synthesis of Cr_2O_3 nanoparticles and their potent anti-bacterial, anti-oxidant and anti-inflammatory activities. *Arab. J. Chem.* **16**, 104544. <https://doi.org/10.1016/j.arabjc.2023.104544> (2023).
26. Santos, C. *et al.* Insights into the Fe^{3+} doping effects on the structure and electron distribution of Cr_2O_3 nanoparticles. *Nanomaterials* **13**, 980. <https://doi.org/10.3390/nano13060980> (2023).
27. Menazea, A. A., El-Newehy, M. H., Thamer, B. M. & El-Naggar, M. E. Preparation of antibacterial film-based biopolymer embedded with vanadium oxide nanoparticles using one-pot laser ablation. *J. Mol. Struct.* **1225**, 129163. <https://doi.org/10.1016/j.molstruc.2020.129163> (2021).
28. Cao, J. *et al.* Constructing stable V_2O_5/V_6O_{13} heterostructure interface with fast Zn^{2+} diffusion kinetics for ultralong lifespan zinc-ion batteries. *J. Colloid Interf. Sci.* **656**, 495–503. <https://doi.org/10.1016/j.jcis.2023.11.127> (2024).
29. Hadi, A. J., Nayef, U. M., Mutlak, F.A.-H. & Jabir, M. S. Enhanced photodetection performance of vanadium pentoxide nanostructures deposited on porous silicon substrate via pulsed laser deposition. *Opt. Quant. Electron.* **56**, 321. <https://doi.org/10.1007/s11082-023-05912-4> (2024).
30. Abd El-Kader, M. F. H., Elabbasy, M. T., Adeboye, A. A., Zeariya, M. G. M. & Menazea, A. A. Morphological, structural and antibacterial behavior of eco-friendly of ZnO/ TiO_2 nanocomposite synthesized via *Hibiscus rosasinensis* extract. *J. Mater. Res. Technol.* **15**, 2213–2220. <https://doi.org/10.1016/j.jmrt.2021.09.048> (2021).
31. Gaabour, L. H. Influence of Cr_2O_3 nanoparticles on the structural, optical, thermal and electrical properties of PEO/CMC nanocomposites. *Opt. Quant. Electron.* **54**, 170. <https://doi.org/10.1007/s11082-022-03565-3> (2022).
32. Awwad, N. S. *et al.* Improvement in electrical conductivity characterization of chitosan/Poly (ethylene oxide) incorporated with V_2O_5 NPs via laser ablation. *J. Mater. Res. Technol.* **16**, 1272–1282. <https://doi.org/10.1016/j.jmrt.2021.12.022> (2022).
33. Hosny, N. M., Samir, G., Zoromba, M. S. & Alghool, S. Poly(o-toluidine dihydrochloride): Spectral characterization and synthesis of eskolite nanoparticles. *Polym.-Plast. Technol. Eng.* **56**(4), 435–442. <https://doi.org/10.1080/03602559.2016.1233256> (2017).
34. El Sayed, A. M. & El-Gamal, S. Synthesis and investigation of the electrical and dielectric properties of $Co_3O_4/(CMC+PVA)$ nanocomposite films. *J. Polym. Res.* **22**, 1–12. <https://doi.org/10.1007/s10965-015-0732-4> (2015).
35. Shamekh, A. M. A., Shaalan, N. M., Hanafy, T. A. & Rashad, M. Linear/nonlinear optical properties of functional inorganic MgO nano-filler in PVA transparent polymer for flexible optoelectronic devices. *Phys. B* **651**, 414617. <https://doi.org/10.1016/j.physb.2022.414617> (2023).
36. El Gohary, H. G. *et al.* Modification and development of optical, thermal, dielectric properties and antibacterial activity of PVA/SA blend by Ag/Se nanofillers: nanocomposites for energy storage devices and food packaging applications. *Polym. Test* **129**, 108258. <https://doi.org/10.1016/j.polymertesting.2023.108258> (2023).
37. Alruwaili, A. & El Sayed, A. M. Characterization and the physical properties of nano-sized Bi_2O_3 /polymer for energy and high-refractive index applications. *Results Phys.* **61**, 107746. <https://doi.org/10.1016/j.rinp.2024.107746> (2024).
38. Parvathi, K. & Ramesan, M. T. Structure, properties and antibacterial behaviour of nickel oxide reinforced natural rubber nanocomposites for flexible electronic applications. *J. Appl. Polym. Sci.* **139**, e53120. <https://doi.org/10.1002/app.53120> (2022).
39. Saber, S., El-Sayed, S. & El Sayed, A. M. Influence of Eu^{3+} on the structural, optical and electrical properties of PEO–PVA: Dual bandgap materials for optoelectronic applications. *J. Mater. Sci. Mater. Electron.* **34**, 406. <https://doi.org/10.1007/s10854-023-09841-6> (2023).
40. Mohammed, G. & El Sayed, A. M. Structural, morphological, optical and dielectric properties of $M^{3+}/PVA/PEG$ SPE Films ($M = La, Y, Fe$ or Ir). *Polym. Adv. Technol.* **30**(3), 698–712. <https://doi.org/10.1002/pat.4508> (2019).

41. Aziz, S. B., Abdullah, O. G. & Rasheed, M. A. A novel polymer composite with a small optical band gap: New approaches for photonics and optoelectronics. *J. Appl. Polym. Sci.* **133**, 44847. <https://doi.org/10.1002/app.44847> (2017).
42. Aziz, S. B. *et al.* Optical properties of pure and doped PVA:PEO based solid polymer blend electrolytes: Two methods for band gap study. *J. Mater. Sci. Mater. Electron.* **28**, 7473–7479. <https://doi.org/10.1007/s10854-017-6437-1> (2017).
43. Hadi, A., Hashim, A. & Al-Khafaji, Y. Structural, optical and electrical properties of PVA/PEO/SnO₂ new nanocomposites for flexible devices. *Trans. Electr. Electron. Mater.* **21**, 283–292. <https://doi.org/10.1007/s42341-020-00189-w> (2020).
44. El Fewaty, N. H., El Sayed, A. M. & Hafez, R. S. Synthesis, structural and optical properties of tin oxide nanoparticles and its CMC/PEG–PVA nanocomposite films. *Polym. Sci. A* **58**(6), 1004–1016. <https://doi.org/10.1134/S0965545X16060055> (2016).
45. Abdelhamied, M. M., Abdelreheem, A. M. & Atta, A. Influence of ion beam and silver nanoparticles on dielectric properties of flexible PVA/PANI Polymer composite films. *Rubber Compos.* **51**(1), 1–12. <https://doi.org/10.1080/14658011.2021.1928998> (2022).
46. Alsulami, Q. A. & Rajeh, A. Synthesis of the SWCNTs/TiO₂ nanostructure and its effect study on the thermal, optical, and conductivity properties of the CMC/PEO blend. *Res. Phys.* **28**, 104675. <https://doi.org/10.1016/j.rinp.2021.104675> (2021).
47. Ramesan Furhan, M. T. Zinc oxide reinforced poly(para-aminophenol) nanocomposites: Structural, thermal stability, conductivity and ammonia gas sensing applications. *J. Macromol. Sci.* **59**, 675–688. <https://doi.org/10.1080/10601325.2022.2111262> (2022).
48. Abdelrazek, E. M., Abdelghany, A. M., Tarabiah, A. E. & Zidan, H. M. AC conductivity and dielectric characteristics of PVA/PVP nanocomposite filled with MWCNTs. *J. Mater. Sci. Mater. Electron.* **30**, 15521–15533. <https://doi.org/10.1007/s10854-019-01929-2> (2019).
49. Suvarna, S., Niranjana, V. S., Subburaj, M. & Ramesan, M. T. Temperature-dependent conductivity, optical properties, thermal stability and dielectric modelling studies of Cu–Al₂O₃/CPE/PVC blend nanocomposites. *Bull. Mater. Sci.* **45**, 246. <https://doi.org/10.1007/s12034-022-02829-8> (2022).
50. Algethami, N., Rajeh, A., Ragab, H. M., Tarabiah, A. E. & Gami, F. Characterization, optical, and electrical properties of chitosan/polyacrylamide blend doped silver nanoparticles. *J. Mater. Sci. Mater. Electron.* **33**, 10645. <https://doi.org/10.1007/s10854-022-08048-5> (2022).
51. Xing, W. *et al.* The similar Cole–Cole semicircles and microwave absorption of hexagonal Co/C composites. *J. Alloys Compd.* **750**, 917–926. <https://doi.org/10.1016/j.jallcom.2018.04.051> (2018).
52. Ragab, H. M. & Rajeh, A. Structural, thermal, optical and conductive properties of PAM/PVA polymer composite doped with Ag nanoparticles for electrochemical application. *J. Mater. Sci. Mater. Electron.* **31**, 16780–16792. <https://doi.org/10.1007/s10854-020-04233-6> (2020).
53. Abutalib, M. M. & Rajeh, A. Influence of ZnO/Ag nanoparticles doping on the structural, thermal, optical and electrical properties of PAM/PEO composite. *Phys. B.* **578**, 9202–0411796. <https://doi.org/10.1016/j.physb.2019.411796> (2020).

Acknowledgements

The authors extend their appreciation to the Deanship of Scientific Research at Northern Border University, Arar, KSA for funding this research work through the project number "NBU-FFR-2024-1512-04".

Author contributions

T.I.A. and A.M.E.S. contributed equally in all parts: writing—original draft, methodology, investigation, formal analysis, data curation, conceptualization.

Competing interests

The authors declare no competing interests.

Additional information

Supplementary Information The online version contains supplementary material available at <https://doi.org/10.1038/s41598-024-62643-6>.

Correspondence and requests for materials should be addressed to A.M.E.S.

Reprints and permissions information is available at www.nature.com/reprints.

Publisher's note Springer Nature remains neutral with regard to jurisdictional claims in published maps and institutional affiliations.



Open Access This article is licensed under a Creative Commons Attribution 4.0 International License, which permits use, sharing, adaptation, distribution and reproduction in any medium or format, as long as you give appropriate credit to the original author(s) and the source, provide a link to the Creative Commons licence, and indicate if changes were made. The images or other third party material in this article are included in the article's Creative Commons licence, unless indicated otherwise in a credit line to the material. If material is not included in the article's Creative Commons licence and your intended use is not permitted by statutory regulation or exceeds the permitted use, you will need to obtain permission directly from the copyright holder. To view a copy of this licence, visit <http://creativecommons.org/licenses/by/4.0/>.

© The Author(s) 2024